A Comparison Between Reactive Potential Fields and Attractor Dynamics

André Carmona Hernandes, Marcelo Becker
School of Engineering of São Carlos
Universidade de São Paulo
São Carlos, Brazil
Email: andre.hernandes@usp.br, becker@sc.usp.br

Jean-Stephane Jokeit, Gregor Schöner
Institut für Neuroinformatik
Ruhr-Universiät Bochum
Bochum, Germany
Email: jean-stephane.jokeit@ini.ruhr-uni-bochum.de,
gregor.schoener@ini.ruhr-uni-bochum.de

***Abstract*—We study four established reactive approaches that can be implemented on computationally weak hardware with the goal of minimizing oscillatory movements to reduce the energetic cost of robot navigation. In this regard, we examine the smoothness and variability of the control action in our analysis. Sensor noise, including the large variance of GPS estimates, is evaluated. Care is taken to make the techniques comparable. Statistical data were obtained in simulation in which environments were randomly varied. We show that the second order Attractor Dynamics Approach satisfies our requirements significantly better than Potential Field approaches.**

I. Introduction

Unmanned Aerial Vehicles (UAVs) are employed in a variety of environments that impose new and challenging design constraints. As a new generation of light-weight robots, UAVs are especially in need of computationally and efficient control since on-board resources are very limited. Conservation of battery energy is directly linked to the range of applicability of the system, but handling the noisy and quickly shifting sensor information that occur in real-world scenarios adds computational burden.

We aim to study the effect of the smoothness of the control action of four reactive techniques. Each is ultimately meant to be embedded into a larger, hybrid architecture, but is considered in isolation in this paper for analysis. The chosen reactive techniques are the Artificial Potential Field approach [1], [2] for robotic manipulators, a variation presented in [3] that is commonly employed for vehicles, the Attractor Dynamics approach, developed by [4] and a variation presented by [9] that modeled human locomotion. These techniques are computationally light-weight while still delivering good results in practice. For UAVs, Potential Fields have been employed (see, for example, [5], [6] for a review) but control actions and noise effects where not considered.

We are specifically interested in studying the the effect of noise in the perception layer. We use simulation experiments in which we may manipulate and analyze the effect of such noise. Further, to better be able to discuss the results of the above methods, we opted to implement the approaches in a two-dimensional, simple vehicle scenario, as this enables comparison to earlier work publications. The outcome of the assessment will guide our future work on UAVs.

We employed an e-Puck mobile robot, a well-known vehicle with actuator dynamics and communication delays 1000 times faster than its implemented control loop. That way, a smoother output control action directly generates a smoother trajectory which will also be more energetically efficient. Finally, as noted in [7], the performance of obstacle avoidance improves with larger range of the sensors, hence we enhanced the sensory range of the e-Puck by emulating noisy ultrasound sensors evenly distributed on its front. The ultrasound range is at least 10 times the robot diameter which is a good range for obstacle avoidance algorithms.

Section II of this paper briefly reviews the implemented variants of the approaches. Section III presents the evaluation methodology including with the metrics used for comparison and a brief discussion of parameter selection. Results are presented in Section IV followed by brief conclusions in Section V.

II. Reactive Algorithms

A. Potential Fields

Although a wide variety of Potential Functions have been presented in the literature, many are really small variations of the original approach customized for specific environments. For this reason, we chose to test the Classical Artificial Potential Field (CAPF) of [1], [2]. We summarize the technique:

$$\vec{F_r} = \vec{F_t} + \vec{F_o} \tag{1}$$

Where $\vec{F_r}$ is the resulting force vector, $\vec{F_t}$ is the target force vector contribution and $\vec{F_o}$ is the resulting obstacles force vector contribution. The $\vec{F_t}$ is defined as shown on Eq. (2):

$$\vec{F_t} = -K_v * (\vec{v} - \nu(\vec{v_d}) * \vec{v_d}) \tag{2}$$

where $\vec{v_d} = K_p * (\vec{T}_{pos} - \vec{R}_{pos})$, $\vec{T}_{pos}$ the target position vector, $\vec{R}_{pos}$, the robot position vector, $\upsilon(\vec{v_d}) = min(1, \frac{1}{\sqrt{\vec{v_d}^2}})$, $\vec{v}$ is the estimated actual velocity vector and K_p and K_v user-defined constants. The $\vec{F_o}$ is defined as shown on Eq. (3):

$$\vec{F_o} = \begin{cases} \eta * (\frac{1}{\rho} - \frac{1}{\rho_0}) * \frac{1}{\rho^2} \cdot \nabla\rho, & \text{if } \rho \leq \rho_0 \\ 0, & \text{otherwise} \end{cases} \tag{3}$$

where ρ is the smallest distance to the obstacle and ρ_0 and η are user-defined constants.

Note, that these equations specify a dynamical system where the end-state is the robot residing in the target position.

In the description of Khatib, Potential Fields yield forces as outputs, but for a non-holonomic robot, such as the e-Puck, the lateral component of the force cannot be exerted on it. We thus chose to interpret, as is commonly done, the forces as being unit-mass and acting as accelerations. We accounted for the angle between the desired acceleration vector and the actual heading as the angular error for a PD-controller which then generated the desired angular rate-of-change. The PD-controller was pre-tuned to avoid oscillations and to not compromise the response time of the method.

B. Potential Fields on Velocity Space

As the Potential Field on Velocity Space (PFVS) we understand the vector field as velocities for the robot. This was described in [3], for example. albeit in a global sense with a known environment and gradient descent search. As we are interested on the reactive usage, we considered the following Field formulation, as described in Eq (4) to Eq. (6):

$$\vec{V_r} = \vec{V_t} + \vec{V_o} \tag{4}$$

$$\vec{V_t} = \begin{cases} K_p * (\vec{T}_{pos} - \vec{R}_{pos}), & \text{if } \rho \leq \rho_T \\ \frac{\rho_T * K_p * (\vec{T}_{pos} - \vec{R}_{pos})}{\rho}, & \text{otherwise} \end{cases} \tag{5}$$

$$\vec{V_o} = \begin{cases} \eta * (\frac{1}{\rho} - \frac{1}{\rho_0}) * \frac{1}{\rho^2} \cdot \nabla\rho, & \text{if } \rho \leq \rho_0 \\ 0, & \text{otherwise} \end{cases} \tag{6}$$

Where $\vec{T}_{pos}$ represents the target position vector, $\vec{R}_{pos}$, the robot position vector, ρ the distance to the obstacle, K_p, ρ_T, η and ρ_0 user-defined constants.

The same transformation from Cartesian vectors to steering commands was performed as for the CAPF approach.

C. First Order Attractor Dynamics

The First Order Attractor Dynamics (FOAD) was first presented in [4] and introduced the notion of the robot performing a task, i.e. moving, while residing in an attractor state of an asymptotically stable dynamical system over a specific variable, one for each task, instead of the attractor state being the final state of the process of all tasks. As it was originally developed for a non-holonomic robot, usage of the steering angle as non-holonomic control variable was directly possible.

The complete set of equations we used can obtained from [8] and the final equations used are presented from Eq. (7) to (11):

$$\dot{\phi} = F_t(\phi) + F_o(\phi) \tag{7}$$

$$F_t(\phi) = -\lambda_t * \sin(\phi - \Psi_t) \tag{8}$$

$$F_o(\phi) = \lambda_o(d_o) * \sin(\phi - \Psi_o) * e^{\left(\frac{-(\phi-\Psi_o)^2}{2\sigma_o(d_o)^2}\right)} \tag{9}$$

$$\lambda_o(d_o) = \beta_3 * e^{\left(\frac{-d_o}{\beta_4}\right)} \tag{10}$$

$$\sigma_o(d_o) = \arctan\left(\tan\left(\frac{\Delta\theta}{2}\right) + \frac{R_{robot}}{R_{robot+d_o}}\right) \tag{11}$$

Where ϕ is the estimated heading angle measured on the Inertial Frame, Ψ_t the angle of the target based on the robot's position measured on the Inertial Frame, similarly for Ψ_o but for the obstacle now, d_o is the distance to the object, R_{robot} is the major radius that involves all the robot, $\Delta\theta$, λ_t, β_3, β_4, are user-defined parameters.

D. Attractor Dynamics with Damping

The Attractor Dynamics with Damping (ADWD) was used by [9] to model human locomotion experiments. It is a second order approach. The Eqs. (12) to (16) describe the technique:

$$\ddot{\phi} = -b * \dot{\phi} + \ddot{\phi}_t + \ddot{\phi}_o \tag{12}$$

$$\ddot{\phi}_t = -K_g * \sin(\phi - \Psi_t)(e^{-c_1 * d_g} + c_2) \tag{13}$$

$$\ddot{\phi}_o = \lambda_o(d_o) * \sin(\phi - \Psi_o) * e^{\left(\frac{-(\phi-\Psi_o)^2}{2\sigma_o(d_o)^2}\right)} \tag{14}$$

$$\lambda_o(d_o) = K_o * e^{\left(\frac{-d_o}{\beta_1}\right)} \tag{15}$$

$$\sigma_o(d_o) = \arctan\left(\tan\left(\frac{\Delta\theta}{2}\right) + \frac{R_{robot}}{R_{robot+d_o}}\right) \tag{16}$$

Where ϕ is the estimated heading angle measured on the Inertial Frame, $\dot{\phi}$ is the estimated angular velocity, Ψ_t the angle of the target based on the robot's position measured on the Inertial Frame, similarly for Ψ_o but for the obstacle now, d_g and d_o are, respectively, the distance to the goal and to the object, R_{robot} is the major radius that involves all the robot, K_g, K_o, b, c_1, c_2, $\Delta\theta$, β_1, are user-defined parameters. Note, that we modified the original equations to include a $\sin$ term and applied an σ_0 as in Eq. (11) to make the approaches more comparable.

III. Experiment Description and Comparison Metrics

A. The Simulated Environment

Our simulations were carried out using the software Webots™ and we chose a sparse forest-like scenario with fifteen slim tree trunks as obstacles for a testbed. We saw the sparse forest scenario as an appropriate environment for these trials for both vehicles and quadrocopter-like UAVs that would mostly operate on a plane parallel to the ground if they were to avoid aggressive, i.e. fast and energy consuming, maneuvers. Moreover, inside forests, GPS signals are extremely noisy and often not reliable, making it a sensible decision to study the limit of the noise effect in this setup.

To make the results comparable over the four approaches, we decided to enforce a forward constant velocity of $0.04m/s$. This implies that for CAPF and PFVS, which are prone to stop at local minima, the robot would tend to move out of these. This modification was termed acceptable, as it was not the focus of our investigations. With a fixed constant velocity, and knowing e-Puck wheel speed limitations, the maximum angular velocity calculated was $3.2rad/s$ at which a saturation cap was applied.

The e-Puck was initially placed beyond the edge of the forest, facing right, and the target waypoint was placed at the other side of the forest. The simulations ran for $50s$ as the robot was not explicitly stopped at the target.

B. Metrics

We used two goal metrics to assess the performance: the minimum distance to any obstacle (M2O) throughout the entire simulation and the minimum distance to target (M2T). The former was a safety measurement, as the larger M2O was, the safer the path was. The latter indicated whether the goal had been reached in the allocated time.

To analyze the control action, we introduced three metrics: The average of angular acceleration (AAA), measured over time. The standard deviation of angular acceleration (SDA), where low values of AAA and SDA would imply smoothness over the entire trajectory. And also the count of occurred saturations (SAT) of the velocity command to capture the capability of the hardware to enact the issued commands.

C. Parameter Estimation

A difficulty of comparisons of different approaches is that performance and comparability relies heavily on the choice of the parameters of the techniques, this being especially true for systems of coupled dynamical equations. Here, one can observe that the approaches do not have the same quantity of parameters and that the parameters not even have the same meaning or the same order of magnitude. Another difficulty is the structure of the parameter space being sparse.

To tackle this issue, we first hand-tuned all the parameters to a qualitatively satisfactory region of parameter space and then applied an optimization using a score-based genetic algorithm. The scores were based on the above mentioned metrics and they were graded using a desired boxplot that express the desired behavior. The truncation selection was chosen with Arithmetic cross-over and small random pertubation as mutation. After 3,200 trials for each technique, the parameters chosen were as follows:

- FOAD: $\lambda_t = 1.1$, $\beta_3 = 3.2$, $\Delta\theta = 0.59$ and $\beta_4 = 0.5$
- ADWD: $K_g = 1.6$, $K_o = 5$, $b = 5.3$, $c1 = 0.23$, $c2 = 0.3$, $\Delta\theta = 0.45$, $\beta_1 = 0.29$
- CAPF: $K_p = 1.1$, $K_v = 5$, $\rho_0 = 0.3$, $\eta = 0.008$
- PFVS: $K_p = 0.8$, $\rho_T = 1$, $\eta = 0.003$, $\rho_0 = 0.2$

In the end, the four techniques did not present collisions, they did not show saturations and they all reached the target area. Thus, the performance metrics showed us that the algorithms achieved with this parameter sets what was expected from them based on the literature.

D. Experiment

We randomly generated 400 forest scenarios with different difficulty levels, Fig. 1 illustrate an easy and hard scenario.

We ran the trials with small and large noises. Trials with small noise served as a ground test. The chosen standard deviations for small noise for the ultrasound and GPS were $1mm$ and $0.14m$, respectively, and large noises were $2cm$ and $0.7m$, respectively. The value of the large noise was determined by searching for the stability margin of the setup. For noisy obstacle data, the stability margin was at a noise level of 29% of the robot diameter, and for the localization of the robot itself, a noise with 10 times the robot diameter delimited the stability margin. The noise in localization position also affected the target representation, for instance, an initial target-robot distance of 1m would erect a desired heading error of $0.6rad$ while when the distance would drop to 0.2m, the error would rise to $1.3rad$.

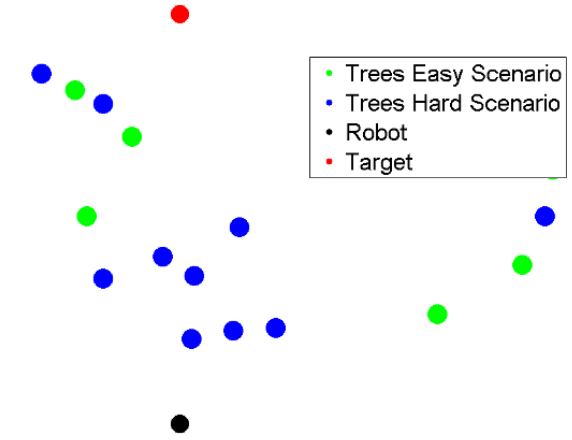

Fig. 1. Superposition of a example of hard scenario and easy scenario generated.

IV. Results

As it postulated by the parameter design, we did not have any collisions for the 800 runs. All achieved the target area and no saturation cap occured. Moreover, all trials achieved similar M2O and M2T metrics overall, with medians $0.08m \pm 0.02m$ and $0.05m \pm 0.05m$, respectively. The figures 2 to 3 show the overall statistics for the control action metrics.

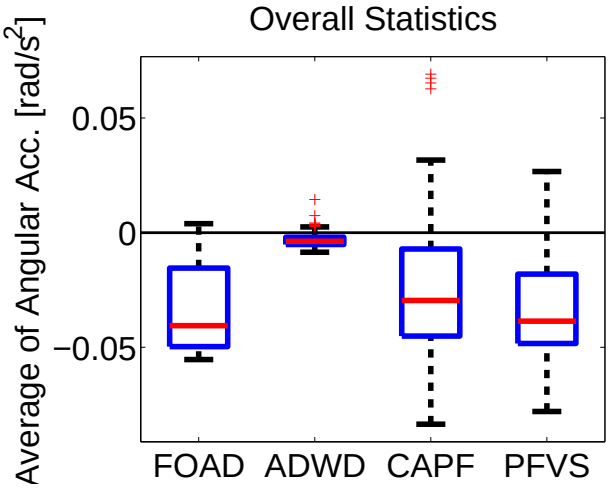

Fig. 2. Boxplot comparison for the four techniques. For the AAA metric, the desired position of the quartiles would be near zero for smoothness.

Note that the plots show the bias of the AAA towards negative values, which comes from the initial orientation of the robot in the experiments.

The ADWD shows the smoothest transitions in control actions and with the lowest variation for the length of the trajectories, even in the presence of noise. The Attractor

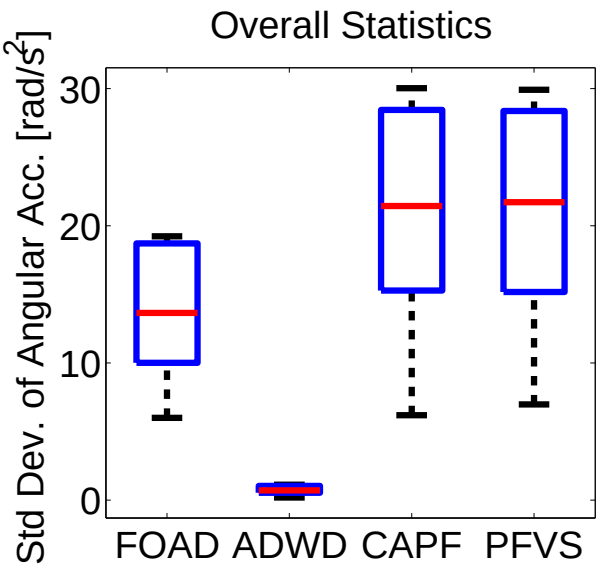

Fig. 3. Boxplot comparison for the four techniques. For the SDA metric, the desired position of the quartiles would be near zero for smoothness.

Dynamics approach tries to hold the system in an attractor state all the time, which only slowly shifts as the robots moves and its AAA and SDA measurements confirm that such a tracking of the attractor was indeed occuring.

The Figures 4 and 5 show how the substantial increase in the localization error affected the performance.

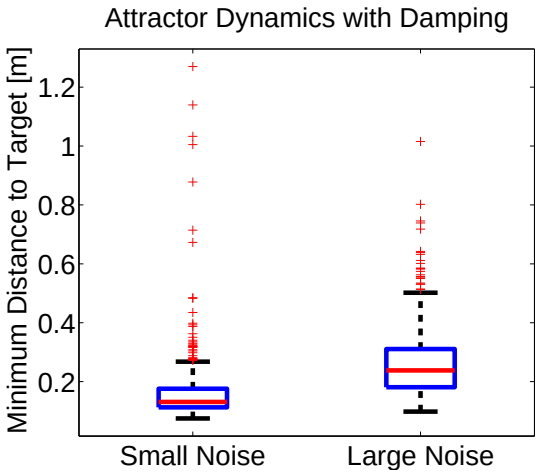

Fig. 4. M2T metric boxplot for ADWD with small and large noise. It was expected higher values for the second quartile and increased difference between first and third quartile due to localization noise affecting target representation.

One may observe, that as the noise in the localization degraded, the M2T metric degraded as would be expected. However ADWD was able to handle significantly more noisy GPS signals and still reach the target. Moreover, the oscillations also increased with larger noise, becoming about twice as big. Nevertheless, while increase on the sensor noise was of a factor of five, the degradation of the smoothness of the trajectory did not occur by the same scale.

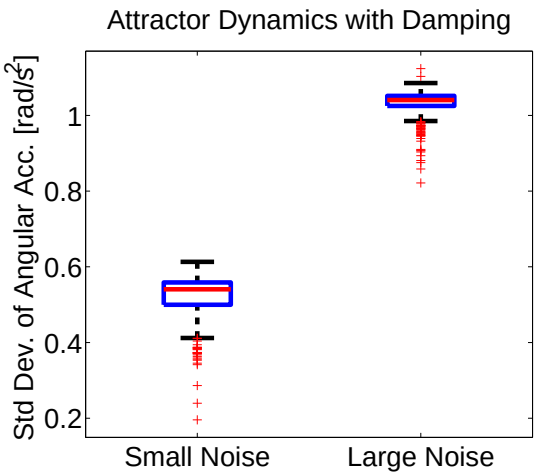

Fig. 5. SDA metric boxplot for ADWD with small and large noise. It was expected a significantly increase in the second quartile due to more oscillations caused by depreciation on target representation.

V. Conclusions and Future Works

We have shown that of the four approaches tested on a variety of sparse forest scenarios, the attractor dynamics with damping exhibited significantly smoother control action while retaining about the same performance. Smoothness on the control action is an important issue since it implies, in real world implementations, that the movement plan is more likely to being followed and the resulting control action is energetically more efficient. In this approach, localization errors up to 10 times the robot's size were tolerable.

Acknowledgment

We would like to thank CAPES for the funding of the grant 99999.014208/2013-00 and RUB/INI for the installations.

References

[1] O. Khatib, Real-time obstacle avoidance for manipulators and mobile robots, The Int. J. of Robotics Research, 1986.

[2] R. C. Arkin, Behavior-Based Robotics, MIT Press, Cambridge, Massachusetts, 1998.

[3] H. Choset, K. M. Lynch, S. Hutchinson, G. A. Kantor, W. Burgard, L. E. Kavraki and S. Thrun, Principles of Robot Motion: Theory, Algorithms and Implementation (Intelligent Robotics and Autonomous Agents series). 2005.

[4] G. Schoener, M. Dose and C. Engels, Dynamics of behavior: Theory and applications for autonomous robot architectures, Robotics and Automatonomous Systems, 1995.

[5] A. Atyabi, D. M. W. Powers, Review of classical and heuristic-based navigation and path planning approaches, Int. J. of Advancements in Computing Technology, vol. 5, no. 14, pp. 114, 2013.

[6] O. Cetim, I. Zagli, G. Yilmaz, Establishing Obstacle and Collision Free Communication Relay for UAVs with Artificial Potential Fields, Journal of Intelligent Robotic Systems, vol. 69, no. 1-4, pp. 361-372, 2013.

[7] M. Becker, R. C. B. Sampaio, S. Bouabdallah, V. Perrot and R. Siegwart, In flight collision avoidance for a micro UAV robot based on onboard sensors, Journal of the Brazilian Society of Mechanical Sciences and Engineering, vol. 3, 2012.

[8] E. Bicho, Dynamic approach to behavior-based robotics, 1999.

[9] B. R. Fajen, W. H. Warren, S. Temizer and L. P. Kaelbling, A dynamical model of visually-guided steering, obstacle avoidance and route selection, Int. J. of Computer Vision, pp. 1334, 2003.